Human Genomics

RESEARCH

Open Access

# Unravelling genetic susceptibility and causal factors in liver health using MRI quantification of inflammation, fat and iron in the liver

Devendra Meena[1,2,3], Michele Pansini[4,5], Alessandro Fichera[6], Jingxian Huang[1,2], Altayeb Ahmed[7], Abbas Dehghan[1,2], Rajarshi Banerjee[6] and Hanieh Yaghootkar[7,8*]

## Abstract

**Background** Liver steatosis, fibroinflammation, and iron overload, are growing global health concerns, yet the genetic architecture and causal pathways linking liver pathology to systemic disease remain incompletely understood.

**Methods** We analysed MRI-derived liver traits—corrected T1 (cT1), proton density fat fraction (PDFF), and liver iron—in 37,626 UK Biobank participants. Genome-wide (GWAS), transcriptome-wide (TWAS), and *cis*-protein Mendelian randomisation (*cis*-MR) analyses were used to identify genes and proteins influencing these traits. We applied two-sample MR to assess bidirectional causal relationships with metabolic and vascular traits and used Multi-Trait Analysis of GWAS (MTAG) to enhance discovery by leveraging genetic correlations.

**Results** GWAS identified 18 loci for cT1, 15 for PDFF, and 5 for liver iron, including six not previously reported. TWAS, *cis*-MR, and proteome-wide analyses prioritised genes (e.g., *FADS1, GPAM, MBOAT7, RAD51C*) and proteins (e.g., RAB2B, GPN1, GSTM4) with putative mechanistic roles. Fine-mapping refined several signals (*GSTM1, TMPRSS6*) to single-variant credible sets. Cell-type enrichment revealed distinct tissue contributions: hepatocytes and intestinal mucosa for cT1, adipose tissue for PDFF, and gastrointestinal tissues for liver iron. MR suggested causal effects of higher liver PDFF and cT1 on obesity-related traits, and inverse genetic associations between liver iron and coronary artery disease. MTAG identified seven additional loci (three for cT1, four for PDFF) not previously reported.

**Conclusions** This integrative imaging-genetics study reveals 13 potentially novel genes and several protein candidates implicated in hepatic steatosis, inflammation, and iron homeostasis. These findings enhance understanding of liver disease biology and may help identify new targets for early detection or treatment.

**Impact and implication** This large imaging-genetics study in over 37,000 people identifies genetic and protein factors linked to liver fat, fibroinflammation, and iron levels. It shows that higher liver fat and inflammation are associated with increased cardiometabolic risk, while higher liver iron appears inversely linked to risk of heart disease. These findings highlight molecular targets such as *FADS1*, *FUT2*, *TMC4*, RAB2B, and GPN1, which could inform future

*Correspondence:
Hanieh Yaghootkar
h.yaghootkar@soton.ac.uk

Full list of author information is available at the end of the article

efforts to improve early detection or treatment of liver disease and its complications in people with obesity or metabolic syndrome.

**Keywords** Magnetic resonance imaging, Genome-wide association study, Mendelian randomisation, Liver cT1, Liver iron, Liver PDFF, Cardiovascular disease

## Introduction

Chronic liver diseases represent a growing global health concern, encompassing a spectrum of conditions such as metabolic dysfunction-associated steatotic liver disease (MASLD, formerly NAFLD) [1, 2], metabolic associated steatohepatitis (MASH), and iron overload syndromes like hereditary haemochromatosis. These diseases affect hundreds of millions of individuals worldwide, with MASLD alone estimated to affect over 25% of the global adult population. If left unrecognised or untreated, these conditions can silently progress to advanced liver fibrosis, cirrhosis, and hepatocellular carcinoma [3]. The rising prevalence of obesity, sedentary lifestyles, and cardiometabolic conditions underscores the urgency of improving early detection and mechanistic understanding of liver pathology [4, 5].

For clinicians and researchers alike, accurate assessment of liver fat accumulation, fibroinflammation, and iron deposition is essential for risk stratification, treatment decisions, and advancing pathophysiological insight [6]. However, traditional diagnostic tools have limitations: liver biopsy, while considered the gold standard, is invasive and unsuitable for large-scale use; circulating liver enzymes are insensitive and nonspecific [2, 7]. Magnetic resonance imaging (MRI) now provides robust, non-invasive quantification of liver tissue properties. Proton density fat fraction (PDFF) measures hepatic fat content; corrected T1 (cT1) reflects fibroinflammatory activity via extracellular fluid; and R2*-based MRI enables quantification of liver iron [8–11]. Together, these imaging biomarkers allow detailed characterisation of liver health at scale.

Parallel to advances in imaging, genome-wide association studies (GWAS) have identified genetic variants associated with individual liver traits [12]. Key discoveries include *PNPLA3* and *TM6SF2* for PDFF and *HFE* and *TMPRSS6* for iron overload [13, 14]. Yet most previous studies have examined these traits in isolation, often relying on smaller sample sizes, or limited to single-omic or univariate approaches. Recent studies using UK Biobank MRI data have made important contributions, but opportunities remain to comprehensively dissect the shared and distinct genetic architecture across liver PDFF, cT1, and iron [13, 15–17]. Moreover, causal inference methods such as Mendelian randomisation (MR) have often been applied separately and in limited scope, without integrating post-GWAS functional analyses across transcriptomic and proteomic layers [18–20]. In particular, multivariate methods such as multi-trait analysis of GWAS (MTAG), and integrative tools such as transcriptome- and proteome-wide association studies, can improve power for discovery and enhance biological interpretation.

Here, we report an integrated analysis of MRI-derived liver traits in 37,626 participants from the UK Biobank. We applied GWAS, MTAG, Bayesian fine-mapping, and functional annotation to map genetic influences on liver cT1, PDFF, and liver iron. To prioritise biologically relevant genes and proteins, we incorporated transcriptomic, proteomic, and cell-type enrichment analyses, and used MR to assess potential causal effects on 17 cardiometabolic and vascular outcomes. This approach enables a detailed exploration of the genetic architecture and systemic consequences of common liver traits and highlights putative molecular targets relevant to early detection and prevention of liver-related complications.

## Methods

### UK biobank participants

This study was conducted using data from the UK Biobank (application number 9914), a prospective cohort of over 500,000 individuals aged 37–73 years at recruitment (99.5% aged 40–69 years), between 2006 and 2010 [21]. All participants provided written informed consent and ethical approval was granted by the North West Multi-Centre Research Ethics Committee (ref: 11/NW/0382).

### Liver imaging acquisition and processing

We utilised quantitative abdominal MRI to assess three clinically relevant liver traits in UK Biobank participants: proton density fat fraction (PDFF, %) for steatosis, hepatic iron concentration (mg/g) and corrected T1 (cT1, ms) as a marker of fibroinflammatory activity. Imaging was conducted at the UK Biobank Imaging Centre in Cheadle, UK, using a Siemens 1.5 T Magnetom Aera scanner, as previously described [13]. Participants were selected based on proximity to imaging sites. PDFF and iron were estimated using a multi-echo spoiled gradient-echo (mGRE) sequence, while T1 times were obtained via a Shortened Modified Look-Locker Inversion Recovery (ShMOLLI) sequence. Both sequences captured a single axial slice at the level of the porta hepatis, acquired during a breath-hold without contrast. This slice-based method has shown strong concordance with histological measures of liver fibrosis, fat, and iron [11]. The slice at the level of the porta hepatis was selected because it

provides a large, homogeneous cross-section of liver parenchyma while avoiding major vessels and has been used consistently in prior validation studies [70]. Previous work has demonstrated strong agreement between single-slice cT1 measurements at this level with histology and predict liver-related outcomes [10, 11]. Potential systematic variability related to body types and respiratory variation is mitigated by standardized breath-hold acquisition, fixed anatomical landmarking, and the use of normalized quantitative MRI metrics rather than relative signal intensities. Residual variability is expected to contribute random noise rather than systematic bias at the population level. The deep learning segmentation approach was previously published in Irving et al. 2017 [22].

Images were processed using LiverMultiScan® Discover 4.0 (Perspectum Ltd, Oxford, UK), which generated parametric maps of PDFF, T2*, and T1. Liver segmentation was performed using the LiverMultiScan (Perspectum Ltd, Oxford, UK) software. The software generates quantitative T2∗, cT1 and PDFF maps and applies an automated liver delineation using a previously published U-net deep-learning model [22], which excludes the major hepatic vessels. The median T2∗value within the segmentation is converted to liver iron concentration and combined with the ShMOLLI T1 data to compute the corrected T1 (cT1) map [11]. R2* values were converted to hepatic iron concentrations, and T1 values were corrected for iron to derive cT1. PDFF was computed as the fat signal fraction relative to the total liver signal. We applied rigorous quality control to exclude scans with artefacts, flawed protocols, mispositioned slices, segmentation failures, or features (e.g., cysts or lesions) that impaired parenchymal quantification. After filtering, 37,651 scans passed quality control. Among these, 37,626 had valid PDFF data, 37,294 had liver iron measurements, and 31,540 had cT1 estimates. All participants included in the final analysis had genotype data and were classified as White European ancestry based on principal component analysis.

#### Genetic association analysis

Detailed protocols for participant genotyping, data collection, and quality control have been previously described [23]. Rigorous quality control procedures were applied to exclude individuals with high genotype missingness, excess heterozygosity, or discrepancies between reported and genetically inferred sex. Participants with a missingness rate > 5% across variants that passed quality control were also excluded. Genotype imputation was performed using two reference panels: the Haplotype Reference Consortium and a combined UK10K/1000 Genomes panel [24, 25]. Only variants with an imputation quality score > 0.3 and a minor allele frequency (MAF) > 1% were retained for analysis.

To identify individuals of White European ancestry, principal components (PCs) derived from the 1000 Genomes reference panel were projected onto the UK Biobank dataset. K-means clustering was then applied to classify participants into ancestry groups, and only those aligning with the European cluster were included in the genetic analyses.

Following image and genotype quality control, liver cT1, liver PDFF, and liver iron measures were available for 31,540, 37,626, and 37,294, individuals, respectively. Genome-wide association analyses were conducted using BOLT-LMM v2.3.4 [26], which models both polygenic and relatedness structures through a linear mixed model approach. The genetic relationship matrix was derived from common (MAF > 5%) genotyped variants passing quality control on both genotyping platforms. Phenotypic traits were inverse-normal transformed prior to analysis, and models were adjusted for age, sex, imaging centre, genotyping array, and principal components for ancestry. Sensitivity analyses adjusting for body mass index (BMI), as well as sex-stratified GWAS, were conducted to explore the robustness of findings and potential sex-specific effects.

Independent loci were defined using a ± 500 kb window around the lead variant and annotated with the nearest protein-coding gene using Ensembl [27]. Conditional analysis was performed using the COnditional and JOint analysis (COJO) implemented in GCTA to identify additional independent signals within loci [28]. A randomly selected subset of 10,000 unrelated White British individuals served as the linkage disequilibrium (LD) reference panel [21]. Secondary signals were retained if they reached genome-wide significance ($P < 5 \times 10^{-8}$) after conditioning on the lead variant.

To further prioritise likely causal variants, we performed Bayesian statistical fine-mapping for each genome-wide significant locus leveraging the approximate Bayes' factor (ABF) method [29]—a single-causal-variant, LD-free fine-mapping method that does not require an LD panel. We chose this approach as it is computationally inexpensive and can be implemented on GWAS summary statistics, without requiring access to individual-level genotype data and a matched reference panel. Future work may incorporate alternative fine-mapping approaches to validate and refine these results; for example, methods such as FINEMAP or SuSiE could be applied to further refine candidate causal variants and assess the presence of multiple causal signals per locus. The analysis was performed using GWAS summary statistics for the selected traits via the easyfinemap pipeline (version 0.4.4; https://jianhua-wang.github.io/easyfinemap/) with default settings for continuous traits without

any reference panel. Briefly, we constructed 95% credible sets (CSs) by calculating Bayes factors and posterior probabilities (PP) for all variants within each region. Variants were ranked by descending PP, and cumulative PPs were summed until the 95% threshold was reached. These credible sets highlight variants most likely to be functionally responsible for the observed genetic associations. We performed GCTA-COJO and fine-mapping independently because they address related but distinct questions. GCTA-COJO was used to reveal secondary signals in loci with complex LD, while fine-mapping was performed to construct 95% credible sets to identify the most likely causal variants at each locus, using the original (unconditioned) marginal summary statistics without a LD reference. This comprehensive framework allowed us to robustly identify novel genetic associations for MRI-derived liver phenotypes and provided a high-resolution map of potential causal variants underpinning liver traits.

#### Genetic correlation

We employed linkage disequilibrium score regression (LDSC) [30] to estimate the genetic correlation between liver imaging-derived phenotypes—proton density fat fraction (PDFF), liver iron, and cT1—and a range of metabolic, cardiovascular, and liver-related traits (supplementary Table 1). LDSC quantifies the shared genetic architecture between two traits by regressing the product of their GWAS Z-scores ($Z_1Z_2$) against LD scores across the genome. The resulting regression slope provides an estimate of genetic correlation, reflecting the degree of genome-wide pleiotropy between the traits.

We conducted the analysis using the publicly available LDSC software (https://github.com/bulik/ldsc), applying pre-computed LD scores derived from European-ancestry samples in the 1000 Genomes reference panel [30]. The analysis was limited to approximately 1.2 million high-quality HapMap3 SNPs, which are known to be reliably imputed across diverse GWAS datasets [31]. GWAS summary statistics were formatted using the munge_sumstats.py script, and regression models were run using ldsc.py. To control for multiple comparisons, we applied Bonferroni correction, considering results to be statistically significant at a threshold of $P < 3.13 \times 10^{-3}$ (0.05/16). This approach enabled a rigorous assessment of the shared genetic basis between liver traits and key clinical outcomes.

#### Two-sample univariable Mendelian randomization (MR)

To assess potential causal relationships between genetically predicted liver traits (cT1, PDFF, and liver iron) and a range of metabolic and clinical outcomes (supplementary Table 1), we conducted two-sample univariable Mendelian randomisation (MR) analyses [32]. We selected independent single nucleotide polymorphisms (SNPs) strongly associated with each liver trait ($P < 5 \times 10^{-8}$), excluding variants with minor allele frequency (MAF) ≤ 5% or F-statistics < 10 to minimise weak instrument bias [33]. Instrument strength was assessed using the F-statistic, calculated as $F = \beta^2/SE^2$, where β denotes the effect estimate for each SNP on the exposure and SE its corresponding standard error. For cT1, F-statistics ranged from 30.05 to 1346.75 (average F-statistics = 149.25). For PDFF, F-statistics ranged from 30.16 to 806.35 and a mean average F-statistic of 169.81. For liver iron, F-statistics ranged from 35.09 to 469.02, with an average F-statistic of 137.04. All minimum F-statistics exceeded the conventional threshold of 10, indicating a relatively low risk of weak instrument bias. To ensure independence among SNPs, we applied linkage disequilibrium (LD) clumping ($r^2 < 0.001$), retaining the variant with the smallest P-value within each locus using the 1000 genomes European data (version 3) as reference panel [25].

Causal estimates for individual SNPs were derived using the Wald ratio method (SNP-outcome effect divided by SNP-exposure effect). These were then aggregated using an inverse-variance weighted (IVW) random-effects model [34], which served as our primary analytic approach. To test the robustness of our findings and account for potential horizontal pleiotropy, we applied weighted median and MR-Egger regression (35) as sensitivity analyses. In addition, we performed the Mendelian Randomization Pleiotropy RESidual Sum and Outlier (MR-PRESSO) test [36] to mitigate potential bias from horizontal pleiotropy. When MR-PRESSO identified possible outliers, we conducted outlier-correction tests, and reported the outlier-corrected causal estimates. Bonferroni correction was used to adjust for multiple comparisons across five sets of MR tests, with statistical significance set at $P < 2.94 \times 10^{-3}$ (0.05/17).

#### *cis*-Mendelian randomisation (*cis*-MR)

We performed *cis*-MR to identify circulating plasma proteins that may mediate the effects of genetic variation on liver phenotypes. We leveraged protein quantitative trait locus (pQTL) data from the UK Biobank Pharma Proteomics Project (UKB-PPP; 2,031 proteins) [37] and deCODE Genetics (1,803 proteins) [38]. For each protein, we selected *cis*-acting variants that were within ± 1 megabase (Mb) of the transcription start site, were genome-wide significant ($P < 5 \times 10^{-8}$) and were not in LD with each other ($r^2 < 0.001$). Steiger filtering was applied to ensure directional consistency [39], retaining only instruments that explained more variance in protein levels than in the liver trait. Causal effects were estimated using the Wald ratio method (for < 2 SNPs) or IVW (for ≥ 2 SNPs). To distinguish true causal effects from confounding due

to LD, we performed a colocalisation analysis using the COLOC package in R [40]. Statistical significance was defined as an FDR-adjusted P-value < 0.05. Associations with a posterior probability of shared causal variant (PPH4) ≥ 0.70 were considered strong evidence of colocalization while those with PPH4 ≥ 0.50 were considered suggestive evidence of colocalization.

#### Transcriptome-wide association study and genetic colocalization

We conducted TWAS [41] to identify genes whose *cis*-regulated expression levels are associated with liver cT1, PDFF, and iron. TWAS was performed using pre-computed expression weights from the GTEx v8 resource [42] and GWAS summary statistics for the liver traits, implemented via the FUSION software framework [41]. Expression-phenotype associations were inferred using a reference panel with paired expression and genotype data.

We focused on ten tissues most relevant to liver biology and metabolism from the GTEx v8 multi-tissue expression datasets, including adipose subcutaneous (N = 581), adipose visceral omentum (N = 469), colon sigmoid (N = 318), kidney cortex (N = 73), liver (N = 208), pancreas (N = 305), small intestine terminal ileum (N = 174), spleen (N = 227), stomach (N = 324), and whole blood (N = 670; http://gusevlab.org/projects/fusion/). Statistical significance was defined as an FDR-adjusted P-value < 0.05. For all nominally significant associations (P < 0.05), we conducted a Bayesian colocalisation analysis to determine whether GWAS and expression quantitative trait locus (eQTL) signals shared a causal variant [40]. We considered a posterior probability for shared causal variant (PPH4) ≥ 0.70 as strong evidence of colocalisation.

#### Summary data-based Mendelian randomisation (SMR)

To further assess whether genetic associations with liver traits were mediated through gene expression, we employed the SMR method [43], combined with the heterogeneity in dependent instruments (HEIDI) test. SMR was applied using liver tissue eQTL data from GTEx v8 [42], integrating SNPs within 1 Mb of transcription start sites and GWAS summary statistics from our BOLT-LMM analyses. The top eQTL ($P < 5 \times 10^{-8}$) for each gene was selected as the instrument. HEIDI tests were used to assess the likelihood that associations were due to a shared causal variant rather than LD (P > 0.05 indicating non-heterogeneity). Analyses were restricted to *cis*-regions by default. Multiple testing was addressed via FDR correction (FDR < 0.05).

#### Tissue and cell-type enrichment analyses

To identify tissues and cell types most relevant to the genetic regulation of liver traits, we applied stratified LD score regression (stratified LDSC) using the –h2-cts flag within the LDSC framework [44]. This approach quantifies the enrichment of trait heritability in genes highly expressed in specific tissues or cell types. We utilised gene expression datasets from GTEx [45] and the Franke lab, which includes RNA-seq profiles from 205 tissues and cell types [44]. Enrichment was considered significant based on partitioned heritability estimates after correcting for multiple testing (FDR < 0.05).

#### Multi-trait analysis of GWAS (MTAG)

Given the well-established genetic correlations between hepatic traits and cardiometabolic diseases, we applied MTAG to improve locus discovery for liver phenotypes. MTAG is a generalised meta-analytic framework that leverages the shared genetic architecture across traits to boost power for identifying trait-specific associations, while accounting for sample overlap and incomplete genetic correlation [46]. By incorporating shared genetic signal with cardiometabolic traits/diseases (e.g., T2D/CAD), MTAG can uncover loci that have weak effects on the liver trait alone but are part of a shared biological pathway with the cardiometabolic disease.

MTAG was run with default parameters, treating PDFF and cT1 as primary traits of interest. To ensure robust inference, we applied strict filtering to prioritise pleiotropic signals likely to reflect true shared biology rather than statistical artefacts. Variants were retained only if they met all of the following criteria:

1. Genome-wide significance in MTAG (pMTAG $P < 5 \times 10^{-8}$);
2. Suggestive association in the original liver GWAS ($P < 5 \times 10^{-6}$) with consistent effect direction; and
3. Evidence of association in the corresponding cardiometabolic trait GWAS (e.g., T2D or CAD).

The post-hoc filtering criteria were deliberately chosen to be stringent to prioritize robust and biologically plausible MTAG associations. Requiring ($P < 5 \times 10^{-6}$) the original GWAS ensured at least moderate single-trait evidence, reducing the risk of spurious MTAG-driven signals, while confirmation of association in the cardiometabolic trait GWAS supported shared biological relevance and minimized false positives. To evaluate potential bias due to violations of the MTAG homogeneity assumption (i.e., variants with null effects on liver traits but strong effects on other traits), we estimated the maximum false discovery rate (MaxFDR), which was 0.03 for PDFF and 0.04 for cT1—well within acceptable limits, indicating robustness of findings.

Significant variants ($P < 5 \times 10^{-8}$) were grouped into loci based on a ± 1 Mb window and annotated to the nearest protein-coding gene. To avoid artefactual

**Table 1** Loci significantly associated with liver traits

| Trait | GWAS model | rsID | CHR | POS | EA | NEA | EAF | BETA | SE | P | N | GENE |
|---|---|---|---|---|---|---|---|---|---|---|---|---|
| cT1 | Univariate GWAS | rs759359281 | 1 | 220,100,497 | CA | C | 0.944 | − 0.126 | 0.017 | 1.10E−13 | 31,540 | *SLC30A10* |
| | | **rs62325476** | **4** | **99,662,849** | **A** | **G** | **0.735** | **− 0.048** | **0.009** | **1.80E−08** | **31,540** | ***TSPAN5*** |
| | | rs13107325 | 4 | 103,188,709 | C | T | 0.930 | − 0.555 | 0.015 | 1.00E−301 | 31,540 | *SLC39A8* |
| | | **rs17269772** | **4** | **105,480,260** | **T** | **C** | **0.978** | **− 0.152** | **0.027** | **8.10E−09** | **31,540** | ***CXXC4*** |
| | | rs79220007 | 6 | 26,098,474 | T | C | 0.929 | 0.141 | 0.015 | 3.00E−20 | 31,540 | *HFE* |
| | | rs13191659 | 6 | 27,001,055 | C | G | 0.916 | 0.081 | 0.014 | 1.10E−08 | 31,540 | *HIST1H2BJ* |
| | | rs1495743 | 8 | 18,273,300 | G | C | 0.222 | − 0.057 | 0.009 | 2.70E−10 | 31,540 | *NAT2* |
| | | rs532436 | 9 | 136,149,830 | G | A | 0.816 | − 0.076 | 0.010 | 9.00E−15 | 31,540 | *ABO* |
| | | rs751229834 | 11 | 61,575,807 | CA | C | 0.690 | − 0.047 | 0.008 | 2.60E−08 | 31,540 | *FADS1,FADS2* |
| | | **rs59372312** | **12** | **51,511,269** | **A** | **G** | **0.933** | **0.093** | **0.016** | **1.70E−09** | **31,540** | ***TFCP2*** |
| | | rs111723834 | 14 | 24,572,932 | G | A | 0.984 | − 0.370 | 0.031 | 7.80E−35 | 31,540 | *NRL,PCK2* |
| | | rs58542926 | 19 | 19,379,549 | C | T | 0.926 | − 0.149 | 0.015 | 1.10E−23 | 31,540 | *TM6SF2* |
| | | rs516246 | 19 | 49,206,172 | C | T | 0.490 | − 0.049 | 0.008 | 2.40E−10 | 31,540 | *FUT2* |
| | | rs6000553 | 22 | 37,469,192 | A | G | 0.465 | 0.071 | 0.008 | 9.50E−21 | 31,540 | *TMPRSS6* |
| | | rs738409 | 22 | 44,324,727 | C | G | 0.786 | − 0.112 | 0.009 | 1.10E−33 | 31,540 | *PNPLA3* |
| | MTAG | rs72662001[a] | 1 | 39,967,280 | T | C | 0.776 | − 0.060 | 0.007 | 7.94E−20 | 68,293 | BMP8A |
| | | rs7012637[b] | 8 | 9,173,209 | G | A | 0.528 | − 0.044 | 0.008 | 1.64E−08 | 33,765 | PPP1R3B |
| | | rs3890483[a] | 19 | 7,220,596 | G | T | 0.560 | − 0.030 | 0.006 | 3.63E−08 | 68,293 | INSR |
| PDFF | Univariate GWAS | **rs140584594** | **1** | **110,232,983** | **A** | **G** | **0.268** | **− 0.046** | **0.008** | **6.50E−09** | **37,651** | ***GSTM1,GSTM2*** |
| | | rs2642438 | 1 | 220,970,028 | A | G | 0.296 | − 0.054 | 0.008 | 1.80E−11 | 37,651 | *MARC1* |
| | | rs1260326 | 2 | 27,730,940 | T | C | 0.394 | 0.061 | 0.007 | 7.30E−19 | 37,651 | *GCKR* |
| | | rs1229984 | 4 | 100,239,319 | T | C | 0.026 | − 0.162 | 0.022 | 1.60E−13 | 37,651 | *ADH1B* |
| | | rs28601761 | 8 | 126,500,031 | C | G | 0.580 | 0.061 | 0.007 | 5.50E−18 | 37,651 | *TRIB1* |
| | | rs7096937 | 10 | 113,950,418 | T | C | 0.270 | 0.058 | 0.008 | 5.30E−13 | 37,651 | *GPAM* |
| | | rs56252442 | 19 | 18,229,208 | G | T | 0.748 | − 0.046 | 0.008 | 1.70E−08 | 37,651 | *MAST3* |
| | | rs58542926 | 19 | 19,379,549 | C | T | 0.926 | − 0.304 | 0.013 | 3.30E−116 | 37,651 | *TM6SF2* |
| | | rs429358 | 19 | 45,411,941 | T | C | 0.849 | 0.120 | 0.010 | 7.10E−36 | 37,651 | *APOE* |
| | | rs11668882 | 19 | 54,675,097 | T | C | 0.561 | − 0.039 | 0.007 | 1.10E−08 | 37,651 | *TMC4* |
| | | rs738408 | 22 | 44,324,730 | C | T | 0.786 | − 0.240 | 0.008 | 4.50E−179 | 37,651 | PNPLA3 |
| | MTAG | rs13389219[a] | 2 | 165,528,876 | C | T | 0.605 | 0.044 | 0.005 | 6.96E−19 | 87,794 | COBLL1 |
| | | rs28650790[b] | 5 | 55,861,464 | C | T | 0.808 | − 0.053 | 0.009 | 9.36E−10 | 44,116 | AC022431.2 |
| | | rs9687846[a] | 5 | 55,861,894 | G | A | 0.799 | − 0.052 | 0.006 | 4.63E−18 | 87,794 | AC022431.2 |
| | | rs741782[b] | 17 | 18,019,712 | T | C | 0.695 | − 0.045 | 0.007 | 1.24E−09 | 44,116 | MYO15A |
| | | rs2315007[a] | 20 | 62,343,845 | T | C | 0.336 | − 0.029 | 0.005 | 1.17E−08 | 87,794 | ZGPAT |

**Table 1** (continued)

| Trait | GWAS model | rsID | CHR | POS | EA | NEA | EAF | BETA | SE | P | N | GENE |
|---|---|---|---|---|---|---|---|---|---|---|---|---|
| Iron | Univariate GWAS | rs4667296 | 2 | 190,517,931 | G | A | 0.228 | − 0.052 | 0.009 | 2.00E−09 | 37,294 | *ASNSD1* |
| | | rs1800562 | 6 | 26,093,141 | G | A | 0.927 | − 0.305 | 0.014 | 7.70E−105 | 37,294 | *HFE* |
| | | **17:56,428,612** | **17** | **56,428,612** | **CAAA** | **C** | **0.526** | **0.047** | **0.008** | **1.60E−09** | **37,294** | ***SUPT4H1*** |
| | | **rs2645490** | **17** | **57,878,509** | **G** | **A** | **0.785** | **0.052** | **0.009** | **5.40E−09** | **37,294** | ***VMP1*** |
| | | rs855791 | 22 | 37,462,936 | A | G | 0.436 | − 0.104 | 0.007 | 1.20E−46 | 37,294 | *TMPRSS6* |

*rsID* reference SNP identifier, *CHR* chromosome, *POS* base-pair position (GRCh build 37), *EA* effect allele, *NEA* non-effect allele, *EAF* effect-allele frequency, *BETA* estimated effect size (per effect allele), *SE* standard error of the effect estimate, *P* p-value for association, *N* sample size, *GENE* nearest gene, Variants shown in bold represent associations not previously reported for these liver traits

[a,b]Genetic variants discovered through multi-trait analysis (MTAG) of liver traits either with type 2 diabetes[a] or coronary artery disease[b], [a] Loci came from bivariate MTAG analysis with T2D; [b] Loci came from bivariate MTAG analysis with CAD

inflation from MTAG-induced correlations, colocalisation analyses were performed using the original single-trait GWAS summary statistics for both the liver trait and cardiometabolic outcome, using the R package coloc as described above. Details of GWAS datasets used are provided in Supplementary Table 1.

## Results

### Characteristics of the liver MRI cohort

The imaging cohort comprised 37,626 participants (18,007 men and 19,619 women). The median age was 66 years for men (interquartile range [IQR]: 59–71) and 64 years for women (IQR: 58–69). Liver cT1 values showed a median of 701 ms (IQR: 669–708) in men and 685 ms (IQR: 565–720) in women. Elevated cT1 values (> 800 ms), indicative of potential liver fibroinflammatory activity, were observed in 6.4% of men (n = 941) and 4.2% of women (n = 665). Liver PDFF, had a median of 3.64% (IQR: 2.53–6.55) in men and 2.59% (IQR: 1.95–4.33) in women. A substantial proportion of participants (35% of men and 21% of women) exceeded the 5% threshold for hepatic steatosis. Median liver iron concentrations were slightly higher in men (1.24 mg/g, IQR: 1.14–1.39) than in women (1.20 mg/g, IQR: 1.11–1.33). Elevated liver iron levels (defined as > 1.8 mg/g) were present in 4.3% of men and 2.3% of women. These results suggest men have higher median levels meaning increased susceptibility to hepatic inflammation, steatosis, and iron overload.

### Liver cT1

Supplementary Fig. 1 provides an overview of the study design and summarizes the main results.

We identified 15 loci associated with cT1, including 12 previously reported (e.g., *PNPLA3, TM6SF2, FADS1, HFE*) and three newly implicated loci: *CXXC4, TFCP2,* and *TSPAN5* (Table 1, Fig. 1, Supplementary Fig. 2–3). The most striking effect was observed for a variant in *SLC39A8* (rs13107325), where individuals carrying the minor allele showed substantially higher cT1 levels (an increase of 0.55 standard deviations (SD); $P = 1 \times 10^{-301}$). These associations remained consistent after accounting for BMI, and we did not observe differences between men and women (supplementary Table 2).

We used fine-mapping techniques to narrow down the list of likely causal variants at several loci, including *SLC39A8* and *TMPRSS6*, to a single candidate variant with high confidence (≥ 95% probability; supplementary Table 3). Enrichment analysis suggested that the strongest genetic signals were active in hepatocytes and intestinal tissues (supplementary Fig. 2). TWAS, which links genetic variation to gene expression in specific tissues, identified 58 unique genes, including *FUT2, FADS1, ABO*, and *NTN5*—all of which showed strong evidence that the same genetic variant influences both

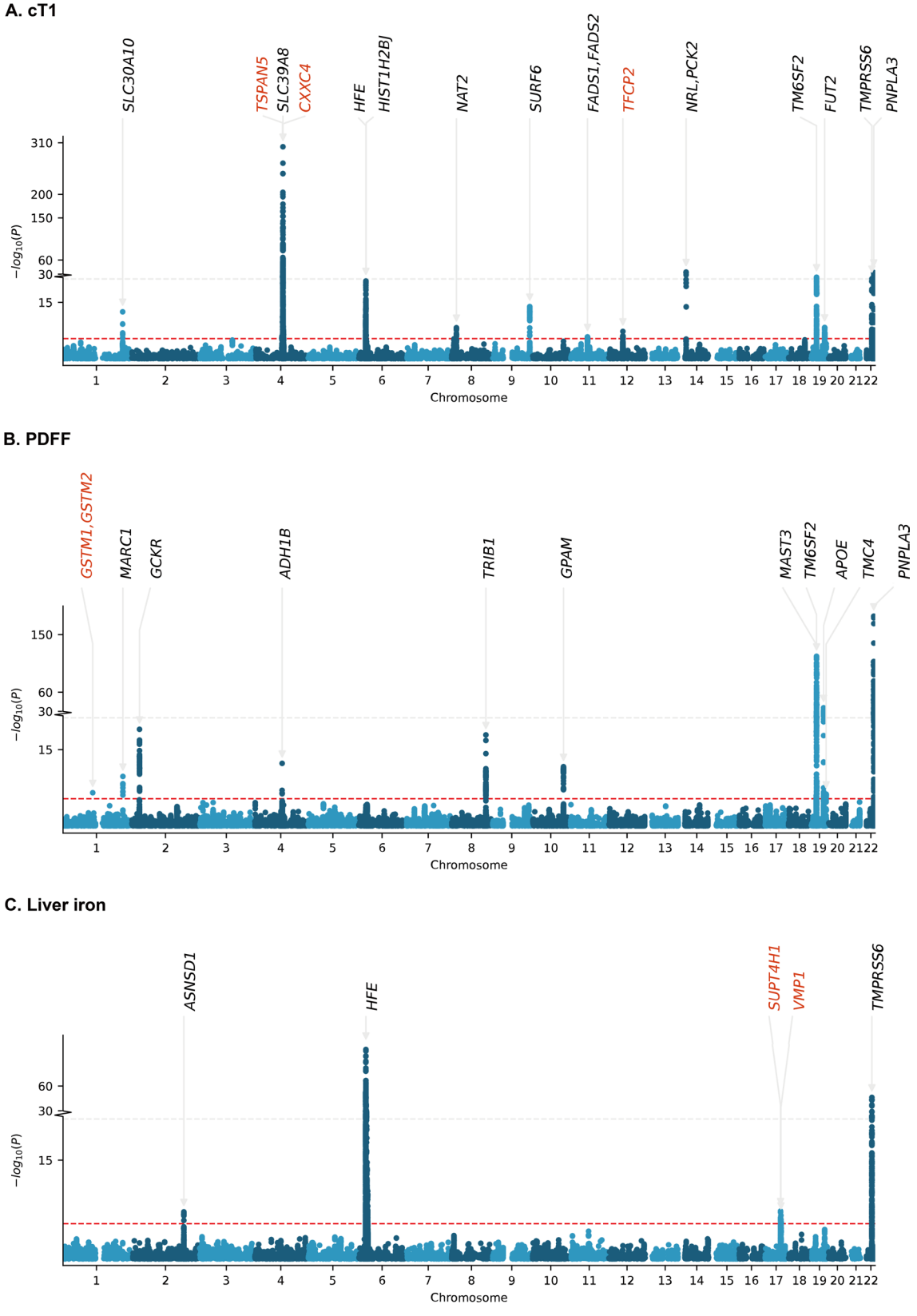


**Fig. 1** Manhattan plots of genome-wide association studies (GWAS) for liver traits. **A**. liver cT1, **B**. liver PDFF, and **C**. liver iron. The horizontal red line indicates the genome-wide significance threshold ($P < 5 \times 10^{-8}$). Nearby genes have been annotated for each lead SNP. Loci highlighted in red represent novel associations not previously reported for these liver traits

gene expression and cT1 (Fig. 2). These findings were further supported by SMR-HEIDI (Fig. 3). We also explored whether blood protein levels could mediate these genetic effects. Using protein-level *cis*-MR, we found that higher circulating levels of ABO and ADH1B proteins were likely to contribute causally to increased cT1, with strong statistical support that the same variants affect both the protein and the liver trait (Fig. 4).

Two-sample MR analyses revealed that genetically higher alanine transaminase (ALT), BMI, WHR, triglycerides, and genetic liability to type 2 diabetes and NAFLD were associated with higher cT1 levels (Fig. 5). In reverse MR, higher genetically predicted cT1 was associated with

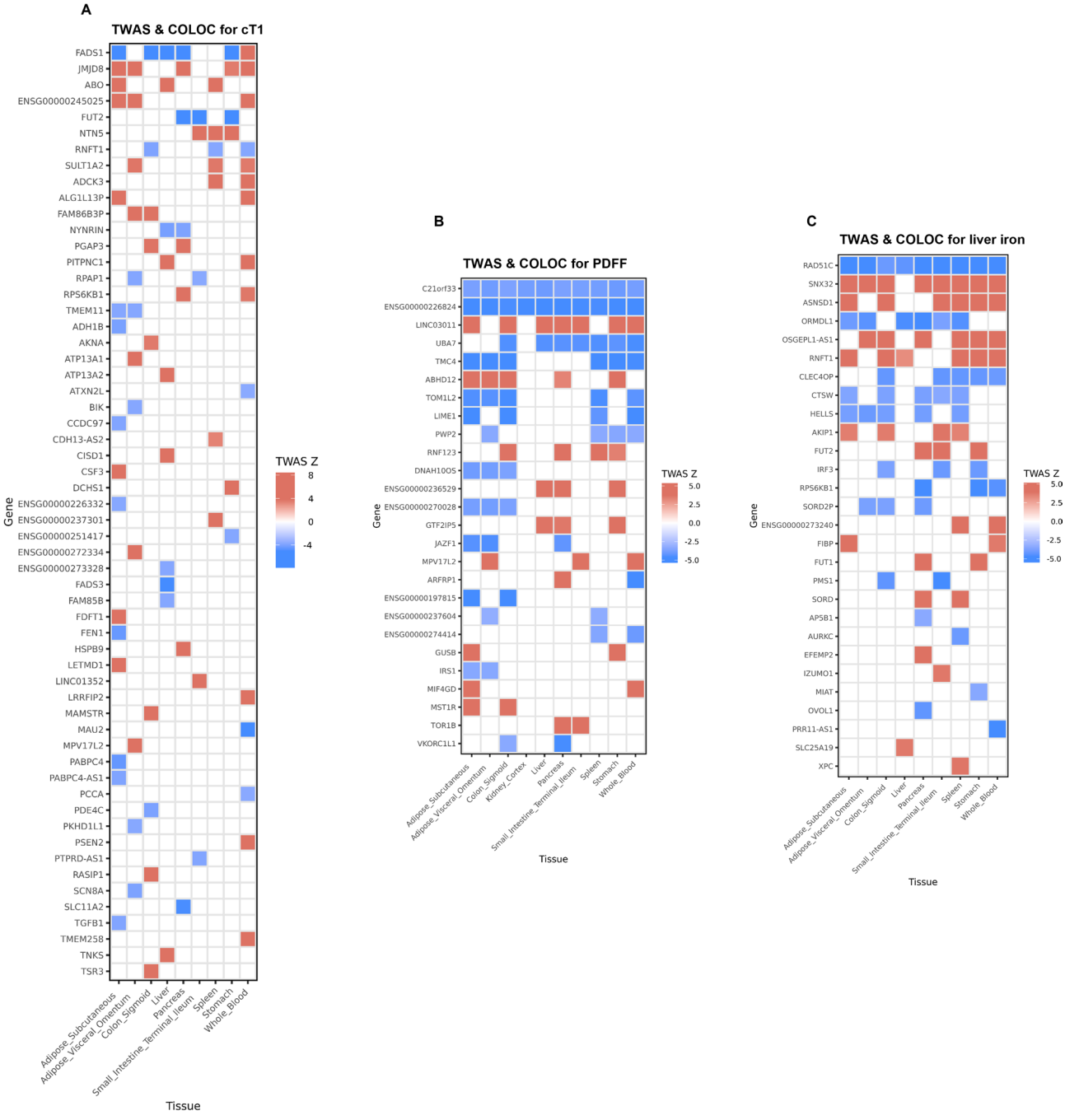


**Fig. 2** Transcriptome-wide association studies (TWAS) and colocalisation analyses for liver traits. Heatmaps display tissue-specific associations for: **A**. liver cT1, **B**. liver PDFF, and **C**. liver iron. Only tissue-specific expression-phenotype associations that were FDR significant (P-TWAS < 0.05) and with strong evidence of sharing the same causal variant (PPH4 ≥ 70%) were highlighted in the heatmap. The colour of the cell represents the direction of the TWAS Z-score

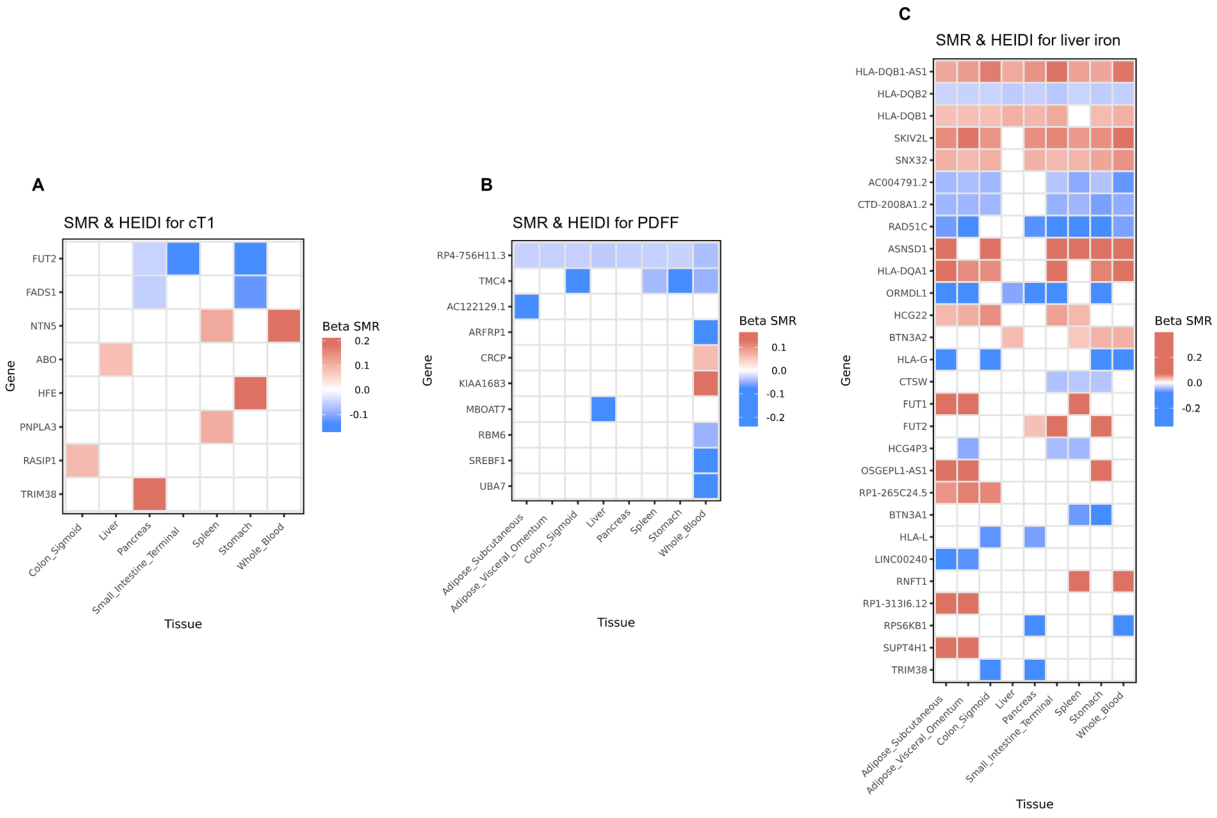


**Fig. 3** SMR and HEIDI analyses highlight putative causal genes for liver traits. Heatmaps display significant gene–trait associations identified through SMR and HEIDI tests for: **A**. liver cT1, **B**. liver PDFF, and **C**. liver iron. Only tissue-specific expression-phenotype associations that were FDR-adjusted $P_{SMR} < 0.05$ and $P_{HEIDI} \geq 0.01$ were highlighted in the heatmap. The colour of the cell represents the direction of the SMR beta estimate

lower HDL-cholesterol and higher BMI (Fig. 5). Detailed estimates for all these analyses of liver cT1 are provided in supplementary tables 4–11.

### Liver PDFF

The GWAS for PDFF confirmed associations with established loci (e.g. *PNPLA3, TM6SF2, GCKR, APOE*) and revealed one novel region near *GSTM1* (rs140584594; $\beta = 0.046$ SD, $P = 6.5 \times 10^{-9}$; Table 1, Fig. 1, supplementary Fig. 3A). The strongest effects were seen for missense variants in *TM6SF2* (rs58542926; $\beta = 0.31$ SD; $p = 6.8 \times 10^{-115}$) and *PNPLA3* (rs738408; $\beta = 0.26$ SD; $p = 4.6 \times 10^{-155}$). These variants were also significantly associated with cT1, showing consistent directions of effect. Adjustment for BMI generally strengthened the associations, and no sex-specific differences were observed (supplementary Table 2). Conditional analysis revealed independent additional signals near *TM6SF2* and *APOE*, and fine-mapping identified putative causal variants (posterior probability ≥ 95%) at several loci, including *APOE*, *SUGP1*, and *GSTM1/2* (supplementary Table 12).

Enrichment analysis highlighted the liver and subcutaneous adipose tissue as the primary cell types involved in the genetic regulation of liver PDFF (supplementary Fig. 2). TWAS identified 63 unique genes (Fig. 2). Of note, lower expression of *C21orf33* and the long non-coding RNA *ENSG00000226824* were consistently associated with higher liver PDFF across all tested tissues. SMR-HEIDI analysis supported 10 unique genes, with overlap observed for *TMC4* between SMR and TWAS results (Fig. 3). Using *cis*-MR, we identified five plasma proteins—RAB2B, APOE, GSTM4, GPN1, and GCKR—as likely causal contributors to liver PDFF, supported by strong colocalisation evidence (PPH4 ≥ 70%; Fig. 4).

Two-sample MR provided robust evidence that genetically predicted increases in BMI, WHR, ALT, gamma-glutamyl transferase (GGT), triglycerides, and liability to type 2 diabetes were causally associated with higher liver PDFF (Fig. 5). In the reverse direction, higher liver PDFF was genetically associated with elevated ALT, increased risk of NAFLD, and higher diastolic blood pressure (Fig. 5). Detailed estimates for all these analyses of liver PDFF are provided in supplementary tables 13–18 (Table 2).

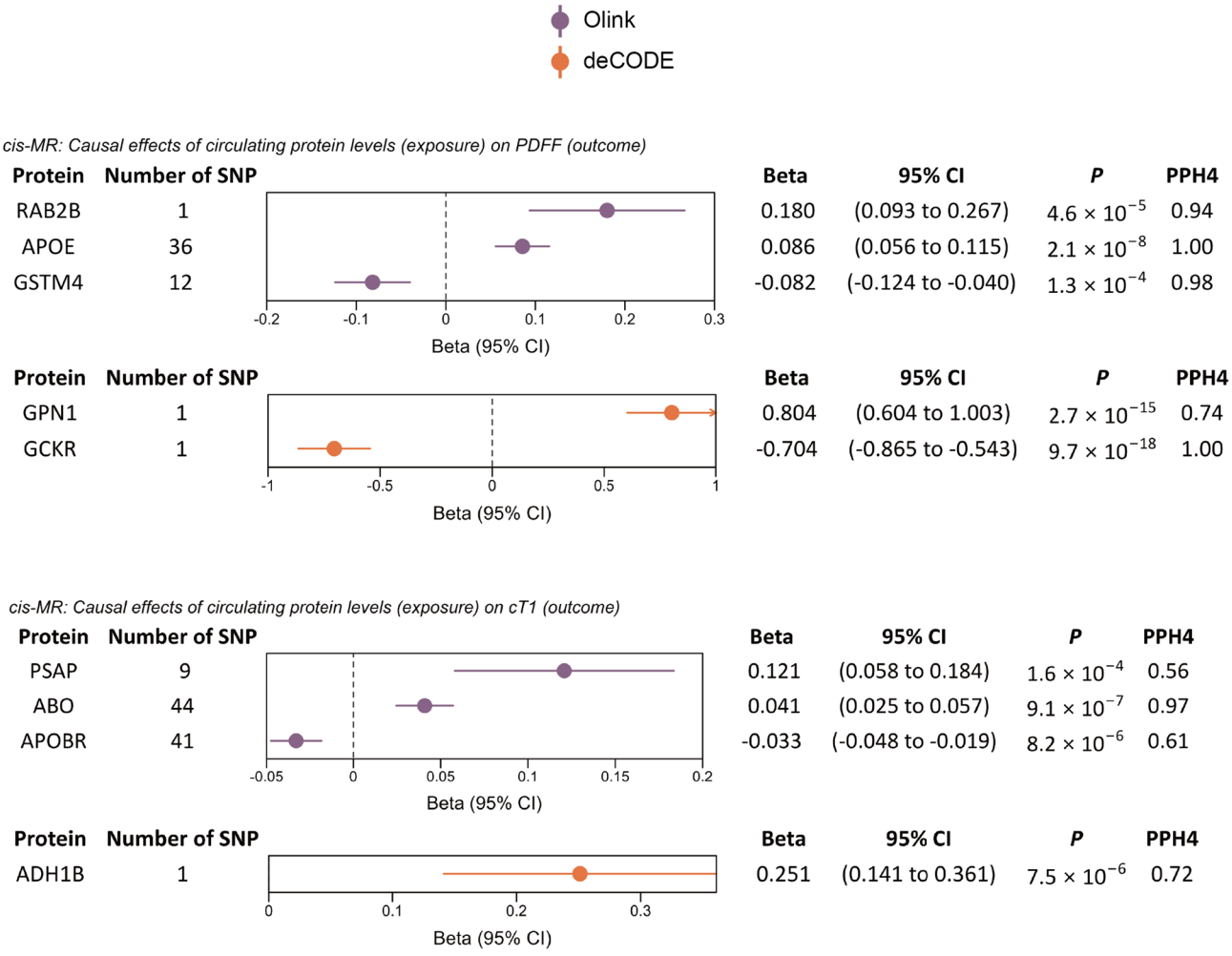


**Fig. 4** *cis*-Mendelian randomization (*cis*-MR) analyses of circulating plasma proteins (from Olink and SomaScan (deCODE) platforms) on liver traits. Top panel: forest plots showing the effect of proteins on PDFF. Bottom panel: Forest plots showing the effect on cT1. Only proteins meeting a 5% FDR threshold and a suggestive Bayesian colocalization posterior probability (H4 > 50%) are displayed. Only proteins with PP.H4 > 0.7 were considered to have strong evidence of colocalization

### Liver iron

The GWAS for liver iron identified five associated loci, including three previously reported regions (*ASNSD1, HFE*, *TMPRSS6*) as well as two newly implicated loci near *VMP1* and *SUPT4H1* (Table 1, Fig. 1, supplementary Fig. 3B). The most prominent signal was observed at the *HFE* locus (rs1800562; 0.31 SD increase per A allele; $p = 7.7 \times 10^{-105}$), a well-known variant associated with hereditary haemochromatosis. These associations were unaffected by adjustment for BMI and were consistent across sexes (supplementary Table 2).

Fine-mapping confirmed rs855791 (*TMPRSS6)* as the likely causal variants (posterior probability ≥ 95%) (Supplementary Table 3). Enrichment analysis suggested that the most relevant tissues for liver iron biology include the liver itself, as well as the small intestine and terminal ileum (supplementary Fig. 2). TWAS identified 28 unique genes whose genetically predicted expression levels were associated with liver iron with strong evidence for inverse associations of *RAD51C* expression with liver iron across most tissues (Fig. 2). SMR-HEIDI further confirmed 45 genes, with overlapping evidence for genes such as *SNX32, RAD51C,* and *ASNSD1* across TWAS and SMR (Fig. 3). In contrast to liver cT1 and PDFF, protein-level *cis*-MR did not identify any circulating proteins with a likely causal role in regulating liver iron.

Two-sample MR demonstrated that genetically higher ALT and GGT were associated with higher liver iron (Fig. 5). In the reverse direction, higher liver iron was linked to lower coronary artery disease risk and lower LDL-C. Although the direction of effect is not straightforward to interpret biologically. We therefore treat this result as a statistically supported genetic association rather than evidence of a protective biological mechanism. Detailed estimates for all these analyses of liver iron are provided in supplementary tables 19–24.

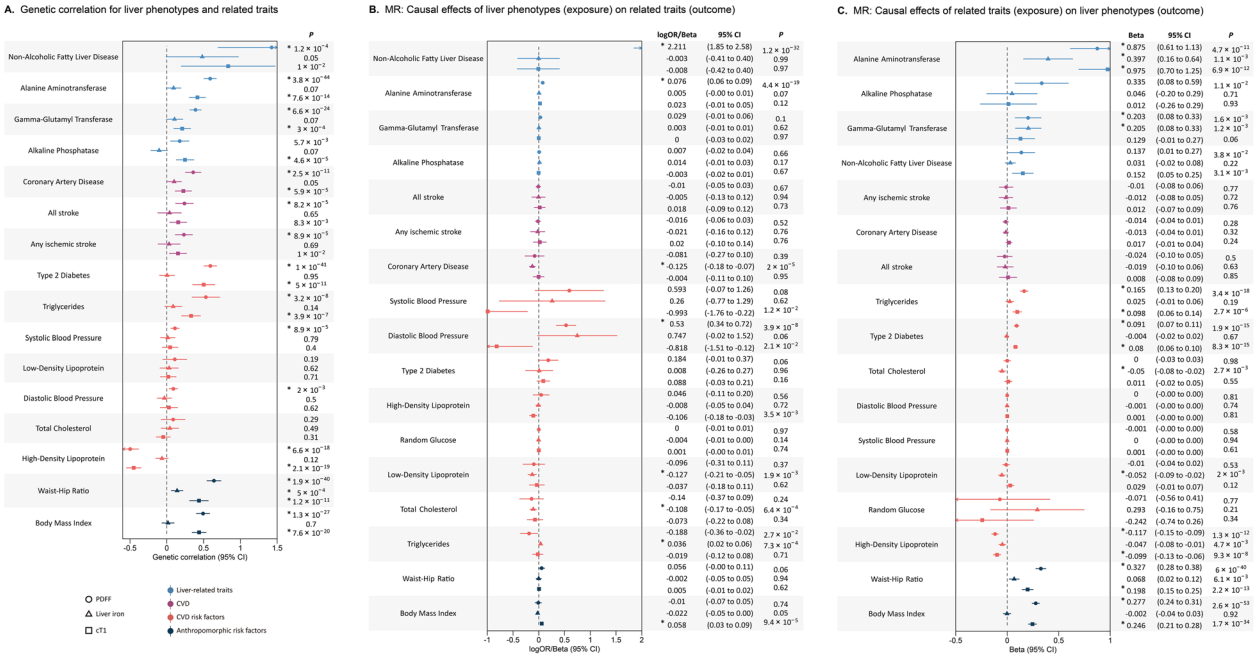


**Fig. 5** Genetic correlation and Mendelian randomisation estimates between liver traits and various cardiometabolic risk factors. **A** forest plot of genetic correlation (rg) results; **B** forest plot of MR estimates for the effect of liver traits on outcomes; and **C**. forest plot of MR estimates for the effect of exposures on liver traits. Genetic correlations and MR estimates that reach the Bonferroni significance level ($3.13 \times 10^{-3}$ for genetic correlations and $P < 2.94 \times 10^{-3}$ for MR estimates) were marked with an asterisk. CI confidence intervals

### Integrated evidence from GWAS, TWAS, *cis*-MR, and SMR–HEIDI

Several loci were supported by multiple complementary lines of evidence, strengthening their candidacy for future functional investigation. Notably, *ABO* was supported by TWAS, SMR and cis-protein MR for CT1. *FADS1/2* and *FUT2* were supported by both TWAS and SMR for cT1, while *ASNSD1* showed support from TWAS and SMR for liver iron. In addition to these multi-method-supported loci, several signals were supported by a single analytical approach. HFE and *PNPLA3* were supported by SMR for cT1, GCKR by cis-protein MR for PDFF, *ADH1B, GPAM*, *MAST3*, and *TMC4* by TWAS for PDFF, and APOE by *cis*-protein MR for PDFF. For liver iron, *SUPT4H1* and *TMPRSS6* were supported by SMR. Together, these findings highlight loci with convergent evidence across methods as well as additional candidates identified through individual approaches.

### Multi-trait analysis identifies novel loci for liver cT1 and PDFF

To increase discovery power beyond single-trait GWAS, we applied MTAG by incorporating genetic summary data from type 2 diabetes, coronary artery disease, and stroke, which showed strong genetic correlations with both liver cT1 and PDFF in our study. Only disease outcomes with LDSC genetic correlation $z > 4$ were included to ensure robust genetic overlap with liver traits. This analysis identified seven additional loci reaching genome-wide significance ($P < 5 \times 10^{-8}$ including variants near or within the genes *BMP8A, INSR*, and *PPP1R3B* associated with liver cT1 and *COBLL1, ZGPAT, MYO15A, AC022431.2, and PPP1R3B* associated with liver PDFF (Table 1, supplementary Fig. 3C–F).

To evaluate whether these associations reflect shared causal variants between liver traits and cardiometabolic disease outcomes, we performed Bayesian colocalisation. We found strong evidence of colocalisation (PPH4 > 70%) at *COBLL1, BMP8A, MYO15A*, and *ZGPAT*, suggesting that a single variant may influence both liver traits and cardiometabolic disease outcomes at these loci. Colocalization results for liver traits and various outcomes are presented in supplementary Table 25.

In follow-up analyses, we also examined the functional relevance of the lead MTAG variants using transcriptomic, metabolomic, and proteomic datasets in the two largest plasma proteogenomic studies [37, 38], 47. For example, rs2315007, the lead variant near *ZGPAT* showed consistently significant effect on liver traits through TWAS *ARFRP1* in pancreas ($\beta = -0.017$, $p = 1.21 \times 10^{-7}$) and *LIME1* in subcutaneous adipose ($\beta = -0.017$, $p = 1.21 \times 10^{-5}$) with strong evidence of colocalization with liver PDFF. This variant acts as a metabolite QTL (mQTL) for indolepropionate (IPA; $\beta = -0.017$, $p = 1.21 \times 10^{-5}$), a microbiome-derived metabolite with hepatoprotective properties [48], and showed strong evidence of colocalization with liver PDFF (PPH4 = 0.98, supplementary Fig. 4). The same variant is a *cis*-protein

**Table 2** Summary of evidence grading across TWAS, *cis*-MR, and SMR–HEIDI analyses for candidate loci

| Trait | rsID | Gene | GWAS Beta | GWAS P | TWAS | SMR HEIDI | *cis* -MR |
|---|---|---|---|---|---|---|---|
| | rs759359281 | *SLC30A10* | -0.126 | 1.10E-13 | | | |
| | **rs62325476** | ***TSPAN5*** | **-0.048** | **1.80E-08** | | | |
| | rs13107325 | *SLC39A8* | -0.555 | 1.00E-301 | | | |
| | **rs17269772** | ***CXXC4*** | **-0.152** | **8.10E-09** | | | |
| | rs79220007 | *HFE* | 0.141 | 3.00E-20 | | | |
| | rs13191659 | *HIST1H2BJ* | 0.081 | 1.10E-08 | | | |
| | rs1495743 | *NAT2* | -0.057 | 2.70E-10 | | | |
| cT1 | rs532436 | *ABO* | -0.076 | 9.00E-15 | | | |
| | rs751229834 | *FADS1,FADS2* | -0.047 | 2.60E-08 | | | |
| | **rs59372312** | ***TFCP2*** | **0.093** | **1.70E-09** | | | |
| | rs111723834 | *NRL,PCK2* | -0.37 | 7.80E-35 | | | |
| | rs58542926 | *TM6SF2* | -0.149 | 1.10E-23 | | | |
| | rs516246 | *FUT2* | -0.049 | 2.40E-10 | | | |
| | rs6000553 | *TMPRSS6* | 0.071 | 9.50E-21 | | | |
| | rs738409 | *PNPLA3* | -0.112 | 1.10E-33 | | | |
| | **rs140584594** | ***GSTM1,GSTM2*** | **-0.046** | **6.50E-09** | | | |
| | rs2642438 | *MARC1* | -0.054 | 1.80E-11 | | | |
| | rs1260326 | *GCKR* | 0.061 | 7.30E-19 | | | |
| | rs1229984 | *ADH1B* | -0.162 | 1.60E-13 | | | |
| | rs28601761 | *TRIB1* | 0.061 | 5.50E-18 | | | |
| PDFF | rs7096937 | *GPAM* | 0.058 | 5.30E-13 | | | |
| | rs56252442 | *MAST3* | -0.046 | 1.70E-08 | | | |
| | rs58542926 | *TM6SF2* | -0.304 | 3.30E-116 | | | |
| | rs429358 | *APOE* | 0.12 | 7.10E-36 | | | |
| | rs11668882 | *TMC4* | -0.039 | 1.10E-08 | | | |
| | rs738408 | PNPLA3 | -0.24 | 4.50E-179 | | | |
| | rs4667296 | *ASNSD1* | -0.052 | 2.00E-09 | | | |
| | rs1800562 | *HFE* | -0.305 | 7.70E-105 | | | |
| Iron | **17:56428612** | ***SUPT4H1*** | **0.047** | **1.60E-09** | | | |
| | **rs2645490** | ***VMP1*** | **0.052** | **5.40E-09** | | | |
| | rs855791 | *TMPRSS6* | -0.104 | 1.20E-46 | | | |

*rsID* reference SNP identifier, *GWAS* genome-wide association study, *BETA* estimated effect size (per effect allele), P p-value for association, *TWAS* Transcriptome-Wide Association Study, *SMR* Summary-data-based Mendelian Randomization, *HEIDI* Heterogeneity in Dependent Instruments, *MR* Mendelian randomisation

QTL (*cis*-pQTL) for TNFRSF6B (Decoy Receptor 3; $p < 1 \times 10^{-300}$ (Fig. 6 and supplementary Fig. 5) and a trans-pQTL for FGFR4. TNFRSF6B and PDFF share a single causal variant in this region as shown by strong colocalization evidence (rs2315007, PPH4 = 0.92; supplementary Fig. 4; supplementary Table 26).

Other variants were also associated with circulating protein abundance relevant to both liver and cardiometabolic traits (supplementary Fig. 6). For liver cT1, rs7012637 (*PPP1R3B*) showed associations with multiple proteins, including CREB3L4, PYGL, BCHE, LEPR, COLGALT1, and CTSB. For liver PDFF, rs13389219 (*COBLL1*) was associated with PLA2R1, LY75, and leptin (LEP), and rs9687846 was associated with IGFBP2, LPL, and LDLR, suggesting this locus may influence hepatic fat accumulation through modulation of lipid metabolism and insulin sensitivity pathways.

## Discussion

This study presents a comprehensive investigation of liver health, leveraging advanced MRI-based phenotyping, large-scale genomic analysis in over 37,000 UK Biobank participants. We simultaneously assess three complementary liver traits including liver inflammation (cT1), steatosis (PDFF), and iron content, mapping both shared and distinct components of their genetic architecture. We expand our understanding of liver health beyond traditional liver function tests and histological proxies, identifying distinct and shared genetic mechanisms across these key hepatic traits. Finally, our comprehensive

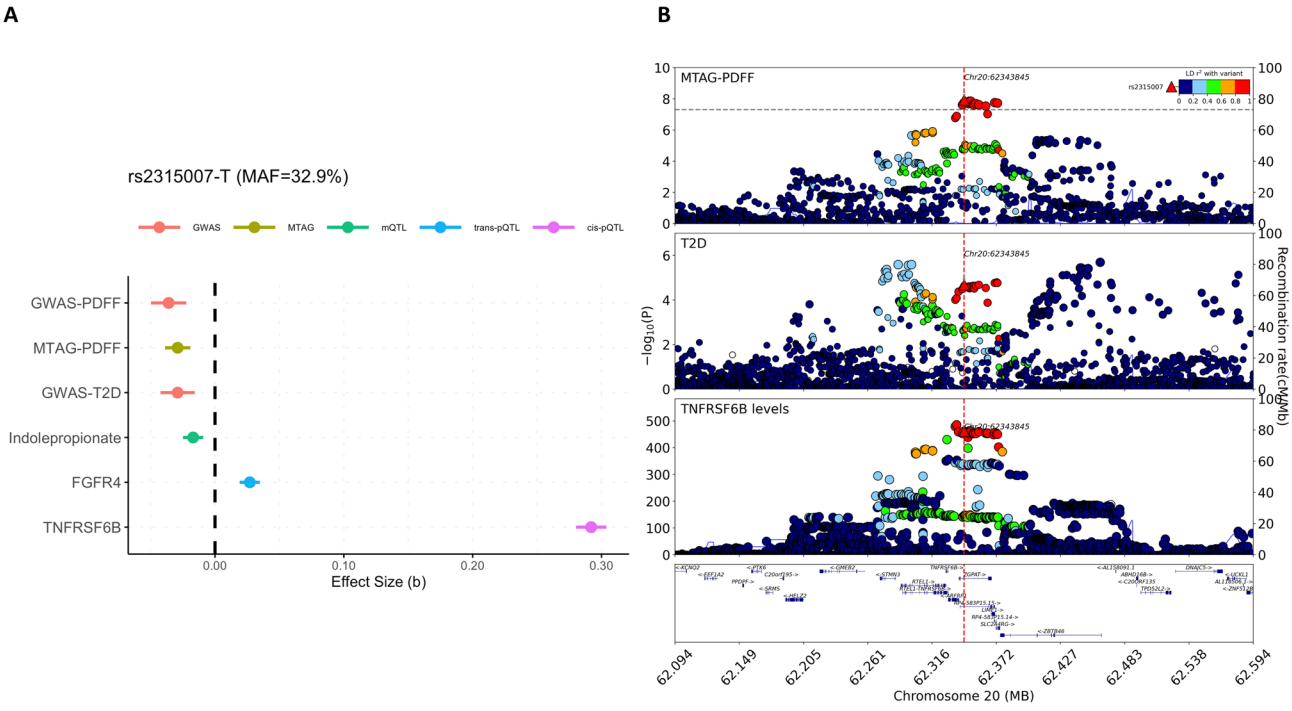


**Fig. 6** Molecular QTL and disease associations for rs2315007-T near ZGPAT. **A** Association of the rs2315007-T allele with GWAS-PDFF, MTAG-PDFF in the current study, indolepropionate from (48), and plasma TNFRSF6B and FGFR4 levels from (37). **B** Stacked regional association plot for the lead MTAG-PDFF variant rs2315007, which colocalizes with the plasma TNFRSF6B cis-pQTL and T2D risk signal in the European population. The color hue represents the strength of r2 indicating the LD structure, as shown in the legend

post-GWAS analyses, leveraging large-scale transcriptomic and proteomic databases, pinpointed genes and proteins associated with these traits and provided novel insights into the biological mechanisms underlying the GWAS signals.

### Genetic architecture and biological insights

Our GWAS confirmed established loci and identified novel associations (e.g., not reported in specific prior large-scale GWAS of the liver MRI traits as in ref 13, 15–17) for each trait. For liver cT1, which reflects fibroinflammatory activity, we identified three new loci, including *CXXC4, TFCP2*, and *TSPAN5*. Fine-mapping analyses pinpointed a high-confidence causal variant in *SLC39A8*, a gene previously linked to metal ion transport and inflammation, reinforcing its potential role in hepatic fibrogenesis. Similarly, *TMPRSS6*, a known regulator of hepcidin and iron homeostasis, was fine-mapped to a single likely causal variant, highlighting its relevance to both cT1 and liver iron biology. In liver PDFF analyses, we refined known associations (e.g. *PNPLA3, TM6SF2, GCKR*) [12], and identified novel signals near *GSTM1/GSTM2*, genes previously associated with liver enzyme levels and metabolic traits [49, 50]. These findings suggest an expanded role for glutathione metabolism and detoxification pathways in hepatic steatosis. Additionally, high-confidence associations were detected at *MARC1, GPAM*, and *TRIB1*, which may influence triglyceride synthesis and liver fat accumulation. For liver iron, novel signals were detected near *ASNSD1, SUPT4H1*, and *VMP1*. *ASNSD1* variants have previously been linked to circulating hepcidin and transferrin receptor levels, suggesting a role in systemic iron regulation and hepatic storage [51].

The MTAG analyses identified seven additional loci. For example, liver cT1 results included *PPP1R3B*, a regulator of hepatic glycogen storage, and *BMP8A*, involved in metabolic thermogenesis, highlighting links between liver inflammation and systemic energy metabolism. The *ZGPAT* locus (rs2315007) for liver PDFF emerged as particularly noteworthy. This variant was associated with PDFF and colocalised with a range of molecular QTLs across transcriptomic (*ARFRP1* and *LIME1*), metabolomic (indolepropionate (IPA)), and proteomic (TNFRSF6B and FGFR4) datasets. Prior research has demonstrated that IPA is a potent anti-non-alcoholic steatohepatitis (NASH) metabolite with hepatoprotective properties [52]. Both TNFRSF6B and FGFR4 are implicated in liver and immune signalling pathways. TNFRSF6B is a soluble receptor that can neutralise the activity of TNFSF members including TL1A (TNFSF15), which has been identified as a susceptibility gene for primary biliary cirrhosis [53, 54]. FGFR4, part of the hepatic FGF19–FGFR4/β-Klotho axis, regulates bile acid synthesis and lipid metabolism, and its activation may reduce

hepatic fat accumulation and suppress gluconeogenic gene expression through an insulin-independent pathway [55]. Rodent studies have shown that *FGFR4* overexpression can prevent hyperlipidaemia, insulin resistance, and fatty liver [56].

TWAS and SMR-HEIDI analyses identified several genes with strong evidence of trait-specific expression effects, many of which have experimentally validated roles in hepatocytes. For cT1, *FUT2, FADS1* and *NTN5* were highlighted. *FADS1* encodes a desaturase highly expressed in hepatocytes and experimentally shown to regulate hepatic lipid composition and inflammation [57, 58]. For PDFF, the *MBOAT7/TMC4* locus stood out and was supported by both transcriptomic approaches. *MBOAT7* is a hepatocyte-expressed acyltransferase whose loss reduces phosphatidylinositol remodelling and promotes steatosis in cellular and mouse models [59, 60], consistent with its observed liver-specific TWAS/SMR signal. For liver iron, *RAD51C* has validated functions in DNA damage responses whose encoded proteins has been shown to promote Hepatitis B virus replication in mice hepatocytes [61]. Several loci prioritised through TWAS and SMR also mapped closely to GWAS sentinel variants. For example, *GPAM*, which encodes the glycerol-3-phosphate acyltransferase 1 (GPAT1) protein and is central to glycerolipid synthesis in hepatocytes [62], was prioritised by SMR in sigmoid colon tissue, and previous research has shown that overexpression of mitochondrial GPAT in rat hepatocytes leads to decreased fatty acid oxidation and increased glycerolipid biosynthesis [62]. Overall, the overlap between TWAS and SMR provides strengthened confidence in these genes as plausible effector transcripts.

TWAS further identified biologically compelling genes that did not reach genome-wide significance in GWAS but showed strong tissue-specific expression associations, including *GUSB* and *SLC25A19* (PDFF), and *LRRFIP2, CSF3* (cT1) and *SNX32* (iron). *LRRFIP2* functions as a macrophage regulator of the NLRP3 inflammasome [63], and its prioritisation for cT1—an inflammation-related measure—is biologically consistent [63, 64]. *CSF3*, a key cytokine controlling granulocyte development and macrophage signalling [65], has demonstrated roles in hepatic inflammatory responses [66]. These findings demonstrate how transcriptomic integration can highlight effector genes involved in lipid metabolism, inflammation and immune–liver cross-talk, even in the absence of strong GWAS signals.

Protein-level MR from large-scale proteomic datasets highlighted biologically plausible proteins—such as ABO, ADH1B, GCKR, GPN1, GSTM4, and RAB2B—as potential upstream drivers of liver phenotype variability. Among these, the novel associations of GPN1 and RAB2B with liver PDFF are worth highlighting. *GPN1* encodes a guanosine triphosphatase enzyme, and RNAi knockdown experiments have shown that it may impact fat accumulation in the liver independently of ethanol exposure in Drosophila models [67]. RAB2B, a member of the Ras protein family, was recently reported to be associated with alcohol-associated hepatitis in an exome-wide association study [68]. These findings suggest a potential role for RAB2B in the molecular mechanisms connecting lipid metabolism and liver inflammation in alcohol-related liver disease. These proteins may serve as future biomarkers or therapeutic targets.

#### Causal inference and metabolic interplay

MR analyses demonstrated that liver phenotypes are not merely passive markers of metabolic dysfunction but participate in bidirectional, and at times divergent, causal relationships. Genetically predicted liver cT1 levels were positively associated with BMI and inversely associated with HDL-C. These results underscore the role of fibroinflammation in the pathophysiology linking adiposity and vascular risk. Liver PDFF was causally influenced by obesity-related traits, including BMI, waist circumference, and triglycerides. In turn, elevated liver PDFF was associated with higher ALT, NAFLD risk, and diastolic blood pressure. These findings reinforce the utility of liver PDFF as an early biomarker of systemic metabolic risk. For liver iron, genetic instruments indicated inverse associations in reverse MR, whereby higher genetically predicted liver iron was linked to lower CAD risk and reduced LDL-C. We emphasise that this finding should not be interpreted as evidence of a clinically protective effect of hepatic iron accumulation. Rather, it likely reflects pleiotropic effects of genetically regulated iron homeostasis pathways—particularly at loci such as *HFE* and *TMPRSS6*—on lipid metabolism, inflammation, or erythropoiesis, rather than a direct causal benefit of increased liver iron per se [69]. In addition, cohort selection, survivor bias, and the cross-sectional nature of MRI-derived liver iron may contribute to non-intuitive directionality. As with all MR findings in complex traits, these results should be viewed as hypothesis-generating and interpreted cautiously pending replication and mechanistic validation.

#### Clinical translation and risk stratification

From a translational standpoint, MRI-derived traits such as cT1 and PDFF, when combined with genetic data, may enable improved risk stratification through polygenic risk scores or integrated imaging–genomics prediction models. Such approaches could refine patient selection for monitoring, early intervention, or trial enrolment in MASLD and related conditions. Several of our findings point to genes and proteins that could serve as potential targets for future pharmacologic modulation. For example, FADS1 is a biologically and chemically tractable

target with active and experimental ligands based on the PHAROS database, suggesting potential for future pharmacologic modulation, while GSTM4 interacts with approved and experimental compounds (cisplatin and POM2-C-HMBP), highlighting its functional relevance and potential as a complementary circulating biomarker. The observed sex differences in liver composition further suggest that future models should incorporate sex-specific thresholds or interactions to improve predictive performance and clinical utility. In current clinical practice, MASLD screening relies on serum scores (such as FIB-4), ultrasound, and selective use of elastography or MRI. Our findings suggest a future workflow where MRI-derived cT1 and PDFF serve as quantitative end points in at-risk individuals (for example, those with type 2 diabetes or obesity), and genetic information helps identify people with a lifelong high burden of steatosis or fibroinflammation who may benefit from earlier imaging or closer follow-up. Variant-informed or polygenic scores could also be integrated into existing cardiometabolic risk calculators. These applications remain exploratory and will require evaluation of clinical utility and cost-effectiveness.

## Strengths and limitations

Key strengths of our study include the use of high-resolution, quantitative MRI phenotypes; robust quality control; and multiple layers of post-GWAS validation, including fine-mapping, transcriptomics, and proteomics. Furthermore, our use of large-scale causal inference frameworks provides mechanistic insights into upstream and downstream consequences of liver trait variation.

Nevertheless, several limitations merit consideration. First, while MRI-derived metrics such as cT1, PDFF, and liver iron are validated non-invasive measures of fibroinflammation, steatosis, and iron content, they do not capture all histological features with the same granularity as liver biopsy. These imaging biomarkers reflect continuous tissue properties rather than discrete histological classifications and should be interpreted within that context.

Second, our analyses were restricted to individuals of European ancestry, which limits generalisability to other populations and prevents formal assessment of ancestry-specific effects. Differences in allele frequencies, LD structure, and environmental exposures across ancestries may affect both locus discovery and the transferability of polygenic risk scores, highlighting the need for future trans-ethnic replication to improve generalizability. As MRI-based liver phenotyping becomes available in more diverse cohorts, it will be important to replicate these findings, perform trans-ethnic fine-mapping, and test whether polygenic scores for cT1, PDFF and liver iron retain predictive performance across ancestries. Such efforts will be essential to ensure that genetically informed risk stratification for liver disease does not exacerbate existing health disparities. Third, our TWAS colocalization analysis (COLOC in FUSION) assumes a single causal variant and therefore cannot capture multiple independent signals; however, the consistently low PPH3 values across prioritized hits suggest the probability of different causal variants between traits is unlikely. Methods accommodating multiple causal variants could be used in future studies. Finally, although MR provides a powerful framework for causal inference, horizontal pleiotropy cannot be entirely excluded.

## Conclusion

Our findings provide a high-resolution map of the genetic landscape underlying three clinically relevant liver traits—cT1, PDFF, and liver iron—and their causal interrelations with cardiometabolic health. The identification of new loci, causal risk factors, and functionally implicated genes and proteins opens new avenues for early detection and personalised intervention in liver disease. Future efforts should extend these findings to diverse ancestries and investigate the translational potential of key molecular mediators identified in this study.

## Supplementary Information

The online version contains supplementary material available at https://doi.org/10.1186/s40246-026-00913-2.

Supplementary Material 1

Supplementary Material 2

### Author contributions

H.Y. and A.D. conceived and designed the study and jointly supervised the overall project. H.Y. conducted the GWAS analyses. D.M., J.H., and A.A. performed the post-GWAS analyses. D.M., A.D., and H.Y. contributed to the interpretation of the analyses and to the development of the analytical strategy and study direction. D.M. and H.Y. drafted the manuscript. M.P., A.F., A.D., and R.B. critically reviewed the manuscript and provided expert input. M.P., A.F., and R.B. contributed to the derivation and processing of the MRI-based liver phenotypes. H.Y. is the guarantor of this work and had full access to all the data in the study and takes responsibility for the integrity of the data and the accuracy of the data analysis.

### Funding

This study was supported by financial support from Diabetes UK (Grant 23/0006598; PI: Hanieh Yaghootkar).

### Data availability

Full data will be returned to UK Biobank and made publicly available via application (amsportal.ukbiobank.ac.uk).

## Declarations

### Ethics approval and consent to participate

This research was conducted using the UK Biobank resource under application number [9914]. UK Biobank has obtained research ethics approval from the North West Multi-centre Research Ethics Committee (REC reference for UK Biobank is 11/NW/0382). All participants provided written informed consent, and the study was conducted in accordance with the principles of the Declaration of Helsinki.

**Competing interests**
The authors declare no competing interests.

**Author details**
[1]Department of Epidemiology and Biostatistics (EBS), School of Public Health, Imperial College London, London, UK
[2]UK Dementia Research Institute, Imperial College London, London, UK
[3]Human Genetics Unit, Indian Statistical Institute, Kolkata, India
[4]Istituto Di Imaging Della Svizzera Italiana (IIMSI), Clinica Di Radiologia EOC, Ente Ospedaliero Cantonale, Via Tesserete 46, 6900 Lugano, Switzerland
[5]Oxford University Hospitals NHS Foundation Trust, Oxford OX3 0AG, UK
[6]Perspectum, Oxford, UK
[7]School of Human Development and Health, Faculty of Medicine, University of Southampton, Southampton, UK
[8]School of Electronics and Computer Science, Faculty of Engineering and Physical Science, University of Southampton, Southampton, UK

Received: 27 October 2025 / Accepted: 7 January 2026
Published online: 28 February 2026

**References**

1. Younossi ZM, Golabi P, Paik JM, Henry A, Van Dongen C, Henry L. The global epidemiology of nonalcoholic fatty liver disease (NAFLD) and nonalcoholic steatohepatitis (NASH): a systematic review. Hepatology. 2023;77(4):1335–47.
2. Harrison SA, Gawrieh S, Roberts K, Lisanti CJ, Schwope RB, Cebe KM, et al. Prospective evaluation of the prevalence of non-alcoholic fatty liver disease and steatohepatitis in a large middle-aged US cohort. J Hepatol. 2021;75(2):284–91.
3. Motta BM, Masarone M, Torre P, Persico M. From non-alcoholic steatohepatitis (NASH) to hepatocellular carcinoma (HCC): epidemiology, incidence, predictions, risk factors, and prevention. Cancers. 2023;15(22):5458.
4. Rinella ME, Neuschwander-Tetri BA, Siddiqui MS, Abdelmalek MF, Caldwell S, Barb D, et al. AASLD practice guidance on the clinical assessment and management of nonalcoholic fatty liver disease. Hepatology. 2023;77(5):1797.
5. Tacke F, Horn P, Wong VWS, Ratziu V, Bugianesi E, Francque S, et al. EASL–EASD–EASO Clinical practice guidelines on the management of metabolic dysfunction-associated steatotic liver disease (MASLD). J Hepatol. 2024;81(3):492–542.
6. Andersson A, Loomba R, Beyer C, Mouchti S, Vuppalanchi R, Harisinghani M, et al. Change in cT1 following interventions in MASLD: a systematic review and meta-analysis. Clin Gastroenterol Hepatol. 2025;18:23.
7. Harrison SA, Dubourg J. Liver biopsy evaluation in MASH drug development: Think thrice, act wise. J Hepatol. 2024;81(5):886–94.
8. Andersson A, Kelly M, Imajo K, Nakajima A, Fallowfield JA, Hirschfield G, et al. Clinical utility of magnetic resonance imaging biomarkers for identifying nonalcoholic steatohepatitis patients at high risk of progression: a multicenter pooled data and meta-analysis. Clin Gastroenterol Hepatol. 2022;20(11):2451-2461.e3.
9. Imajo K, Honda Y, Yoneda M, Saito S, Nakajima A. Magnetic resonance imaging for the assessment of pathological hepatic findings in nonalcoholic fatty liver disease. J Med Ultrasonics. 2020;47(4):535–48.
10. Pavlides M, Banerjee R, Tunnicliffe EM, Kelly C, Collier J, Wang LM, et al. Multiparametric magnetic resonance imaging for the assessment of non-alcoholic fatty liver disease severity. Liver Int. 2017;37(7):1065–73.
11. Banerjee R, Pavlides M, Tunnicliffe EM, Piechnik SK, Sarania N, Philips R, et al. Multiparametric magnetic resonance for the non-invasive diagnosis of liver disease. J Hepatol. 2014;60(1):69–77.
12. Ahmed A, Cule M, Bell JD, Sattar N, Yaghootkar H. Differing genetic variants associated with liver fat and their contrasting relationships with cardiovascular diseases and cancer. J Hepatol. 2024;81(6):921–9.
13. Parisinos CA, Wilman HR, Thomas EL, Kelly M, Nicholls RC, McGonigle J, et al. Genome-wide and Mendelian randomisation studies of liver MRI yield insights into the pathogenesis of steatohepatitis. J Hepatol. 2020;73(2):241–51.
14. Wilman HR, Parisinos CA, Atabaki-Pasdar N, Kelly M, Thomas EL, Neubauer S, et al. Genetic studies of abdominal MRI data identify genes regulating hepcidin as major determinants of liver iron concentration. J Hepatol. 2019;71(3):594–602.
15. Liu Y, Basty N, Whitcher B, Bell JD, Sorokin EP, van Bruggen N, et al. Genetic architecture of 11 organ traits derived from abdominal MRI using deep learning. Elife. 2021;15(10):e65554.
16. O'Dushlaine C, Germino M, Verweij N, Nielsen JB, Yadav A, Benner C, et al. Genome-wide association study of liver fat, iron, and extracellular fluid fraction in the UK Biobank. medRxiv. 2021. https://doi.org/10.1101/2021.10.25.21265127v1.
17. Ahmad S, Carrasquilla GD, Langner T, Menzel U, Ahmad N, Sayols-Baixeras S, et al. Impact of genetic variants linked to liver fat and liver volume on MRI-mapped body composition. JHEPReport. 2025;7(9):12.
18. Ni Y, Wang W, Liu Y, Jiang Y. Causal associations between liver traits and Colorectal cancer: a Mendelian randomization study. BMC Med Genomics. 2023;16(1):316.
19. Wang K, Yang F, Zhang P, Yang Y, Jiang L. Genetic effects of iron levels on liver injury and risk of liver diseases: a two-sample Mendelian randomization analysis. Front Nutr. 2022. https://doi.org/10.3389/fnut.2022.964163/full.
20. Wu H, Zhou D, Zhu J, Tu J. Causal relationship analysis of MRI measurements of major human internal organs and liver disease. Eur J Med Res. 2025;30(1):268.
21. Bycroft C, Freeman C, Petkova D, Band G, Elliott LT, Sharp K, et al. The UK biobank resource with deep phenotyping and genomic data. Nature. 2018;562(7726):203–9.
22. Irving B, Hutton C, Dennis A, Vikal S, Mavar M, Kelly M, et al. Deep quantitative liver segmentation and vessel exclusion to assist in liver assessment. In: Valdés Hernández M, González-Castro V, editors., et al., medical image understanding and analysis. Cham: Springer International Publishing; 2017. p. 663–73.
23. Sudlow C, Gallacher J, Allen N, Beral V, Burton P, Danesh J, et al. UK biobank: an open access resource for identifying the causes of a wide range of complex diseases of middle and old age. PLoS Med. 2015;12(3):e1001779.
24. Walter K, Min JL, Huang J, Crooks L, Memari Y, et al. The UK10K project identifies rare variants in health and disease. Nature. 2015;526(7571):82–90.
25. Genomes Project Consortium, Auton A, Brooks LD, Durbin RM, Garrison EP, Kang HM, et al. A global reference for human genetic variation. Nature. 2015;526(7571):68–74.
26. Loh PR, Tucker G, Bulik-Sullivan BK, Vilhjálmsson BJ, Finucane HK, Salem RM, et al. Efficient Bayesian mixed-model analysis increases association power in large cohorts. Nat Genet. 2015;47(3):284–90.
27. Dyer SC, Austine-Orimoloye O, Azov AG, Barba M, Barnes I, Barrera-Enriquez VP, et al. Ensembl 2025. Nucleic Acids Res. 2025;53(D1):D948–57.
28. Yang J, Ferreira T, Morris AP, Medland SE. 2012. Genetic Investigation of ANthropometric Traits (GIANT) Consortium DIAbetes Genetics Replication And Meta-analysis (DIAGRAM) Consortium, Conditional and joint multiple-SNP analysis of GWAS summary statistics identifies additional variants influencing complex traits. Nat Genet. 44(4):369–75, S1–3.
29. Asimit JL, Hatzikotoulas K, McCarthy M, Morris AP, Zeggini E. Trans-ethnic study design approaches for fine-mapping. Eur J Hum Genet. 2016;24(9):1330–6.
30. Bulik-Sullivan B, Finucane HK, Anttila V, Gusev A, Day FR, Loh PR, et al. An atlas of genetic correlations across human diseases and traits. Nat Genet. 2015;47(11):1236–41.
31. Altshuler DM, Gibbs RA, Peltonen L, Altshuler DM, Gibbs RA, et al. Integrating common and rare genetic variation in diverse human populations. Nature. 2010;467(7311):52–8.
32. Hartwig FP, Davies NM, Hemani G, Davey SG. Two-sample Mendelian randomization: avoiding the downsides of a powerful, widely applicable but potentially fallible technique. Int J Epidemiol. 2016;45(6):1717–26.
33. Burgess S, Thompson SG, CRP CHD Genetics Collaboration. Avoiding bias from weak instruments in Mendelian randomization studies. Int J Epidemiol. 2011;40(3):755–64.
34. Burgess S, Butterworth A, Thompson SG. Mendelian randomization analysis with multiple genetic variants using summarized data. Genet Epidemiol. 2013;37(7):658–65.
35. Bowden J, Davey Smith G, Burgess S. Mendelian randomization with invalid instruments: effect estimation and bias detection through egger regression. Int J Epidemiol. 2015;44(2):512–25.
36. Verbanck M, Chen CY, Neale B, Do R. Detection of widespread horizontal pleiotropy in causal relationships inferred from Mendelian randomization between complex traits and diseases. Nat Genet. 2018;50(5):693–8.
37. Sun BB, Chiou J, Traylor M, Benner C, Hsu YH, Richardson TG, et al. Plasma proteomic associations with genetics and health in the UK Biobank. Nature. 2023;622(7982):329–38.

38. Ferkingstad E, Sulem P, Atlason BA, Sveinbjornsson G, Magnusson MI, Styrmisdottir EL, et al. Large-scale integration of the plasma proteome with genetics and disease. Nat Genet. 2021;53(12):1712–21.
39. Hemani G, Tilling K, Smith GD. Orienting the causal relationship between imprecisely measured traits using GWAS summary data. PLoS Genet. 2017;13(11):e1007081.
40. Giambartolomei C, Vukcevic D, Schadt EE, Franke L, Hingorani AD, Wallace C, et al. Bayesian test for colocalisation between pairs of genetic association studies using summary statistics. PLoS Genet. 2014;10(5):e1004383.
41. Gusev A, Ko A, Shi H, Bhatia G, Chung W, Penninx BWJH, et al. Integrative approaches for large-scale transcriptome-wide association studies. Nat Genet. 2016;48(3):245–52.
42. GTEx Consortium. 2020. The GTEx Consortium atlas of genetic regulatory effects across human tissues. Science. 11: 369(6509):1318–30.
43. Zhu Z, Zhang F, Hu H, Bakshi A, Robinson MR, Powell JE, et al. Integration of summary data from GWAS and eqtl studies predicts complex trait gene targets. Nat Genet. 2016;48(5):481–7.
44. Finucane HK, Reshef YA, Anttila V, Slowikowski K, Gusev A, Byrnes A, et al. Heritability enrichment of specifically expressed genes identifies disease-relevant tissues and cell types. Nat Genet. 2018;50(4):621–9.
45. GTEx Consortium. Human genomics. The genotype-tissue expression (GTEx) pilot analysis: multitissue gene regulation in humans. Science. 2015;348(6235):648–60.
46. Turley P, Walters RK, Maghzian O, Okbay A, Lee JJ, Fontana MA, et al. Multi-trait analysis of genome-wide association summary statistics using MTAG. Nat Genet. 2018;50(2):229–37.
47. Arnold M, Raffler J, Pfeufer A, Suhre K, Kastenmüller G. SNiPA: an interactive, genetic variant-centered annotation browser. Bioinformatics. 2015;31(8):1334–6.
48. Shin SY, Fauman EB, Petersen AK, Krumsiek J, Santos R, Huang J, et al. An atlas of genetic influences on human blood metabolites. Nat Genet. 2014;46(6):543–50.
49. Pazoki R, Vujkovic M, Elliott J, Evangelou E, Gill D, Ghanbari M, et al. Genetic analysis in European ancestry individuals identifies 517 loci associated with liver enzymes. Nat Commun. 2021;12(1):2579.
50. Huang J, Huffman JE, Huang Y, Do Valle Í, Assimes TL, Raghavan S, et al. Genomics and phenomics of body mass index reveals a complex disease network. Nat Commun. 2022;13(1):7973.
51. Allara E, Bell S, Smith R, Keene SJ, Gill D, Gaziano L, et al. Novel loci and biomedical consequences of iron homoeostasis variation. Commun Biol. 2024;7(1):1631.
52. Zhao ZH, Xin FZ, Xue Y, Hu Z, Han Y, Ma F, et al. Indole-3-propionic acid inhibits gut dysbiosis and endotoxin leakage to attenuate steatohepatitis in rats. Exp Mol Med. 2019;51(9):1–14.
53. Nakamura M, Nishida N, Kawashima M, Aiba Y, Tanaka A, Yasunami M, et al. Genome-wide association study identifies TNFSF15 and POU2AF1 as susceptibility loci for primary biliary cirrhosis in the japanese population. Am J Hum Genet. 2012;91(4):721–8.
54. Aiba Y, Harada K, Komori A, Ito M, Shimoda S, Nakamura H, et al. Systemic and local expression levels of TNF-like ligand 1A and its decoy receptor 3 are increased in primary biliary cirrhosis. Liver Int. 2014;34(5):679–88.
55. Potthoff MJ, Boney-Montoya J, Choi M, He T, Sunny NE, Satapati S, et al. FGF15/19 regulates hepatic glucose metabolism by inhibiting the CREB-PGC-1α pathway. Cell Metab. 2011;13(6):729–38.
56. Huang X, Yang C, Luo Y, Jin C, Wang F, McKeehan WL. FGFR4 prevents hyperlipidemia and insulin resistance but underlies high-fat diet induced fatty liver. Diabetes. 2007;56(10):2501–10.
57. Ghooray DT, Xu M, Shi H, McClain CJ, Song M. Hepatocyte-specific Fads1 overexpression attenuates western diet-induced metabolic phenotypes in a rat model. Int J Mol Sci. 2024;25(9):4836.
58. Athinarayanan S, Fan YY, Wang X, Callaway E, Cai D, Chalasani N, et al. Fatty acid desaturase 1 influences hepatic lipid homeostasis by modulating the PPARα-FGF21 axis. Hepatol Commun. 2021;5(3):461–77.
59. Anderson KE, Kielkowska A, Durrant TN, Juvin V, Clark J, Stephens LR, et al. Lysophosphatidylinositol-acyltransferase-1 (LPIAT1) is required to maintain physiological levels of PtdIns and PtdInsP(2) in the mouse. PLoS ONE. 2013;8(3):e58425.
60. Mancina RM, Dongiovanni P, Petta S, Pingitore P, Meroni M, Rametta R, et al. The MBOAT7-TMC4 variant rs641738 increases risk of nonalcoholic fatty liver disease in individuals of European descent. Gastroenterology. 2016;150(5):1219-1230.e6.
61. Peng TW, Ma QF, Li J, Wang X, Zhang CH, Ma J, et al. HBV promotes its replication by up-regulating RAD51C gene expression. Sci Rep. 2024;14(1):2607.
62. Lindén D, William-Olsson L, Rhedin M, Asztély AK, Clapham JC, Schreyer S. Overexpression of mitochondrial GPAT in rat hepatocytes leads to decreased fatty acid oxidation and increased glycerolipid biosynthesis. J Lipid Res. 2004;45(7):1279–88.
63. Jin J, Yu Q, Han C, Hu X, Xu S, Wang Q, et al. LRRFIP2 negatively regulates NLRP3 inflammasome activation in macrophages by promoting Flightless-I-mediated caspase-1 inhibition. Nat Commun. 2013;4:2075.
64. Patankar JV, Wong CK, Morampudi V, Gibson WT, Vallance B, Ioannou GN, et al. Genetic ablation of Cyp8b1 preserves host metabolic function by repressing steatohepatitis and altering gut microbiota composition. Am J Physiol Endocrinol Metab. 2018;314(5):E418–32.
65. Buniello A, MacArthur JAL, Cerezo M, Harris LW, Hayhurst J, Malangone C, et al. The NHGRI-EBI GWAS Catalog of published genome-wide association studies, targeted arrays and summary statistics 2019. Nucleic Acids Res. 2019;47(D1):D1005–12.
66. Huang XY, Yang D, Liu YZ, Zhang EX, Yang Q, Kang W, et al. SETDB1 promotes mammalian liver regeneration by stimulating cytokine CSF3 in hepatocytes. Cell Rep. 2025;44(6):115843.
67. O'Farrell F, Aleyakpo B, Mustafa R, Jiang X, Pinto RC, Elliott P, et al. Evidence for involvement of the alcohol consumption WDPCP gene in lipid metabolism, and liver cirrhosis. Sci Rep. 2023;13(1):20616.
68. Yuan Q, Hodgkinson C, Liu X, Barton B, Diazgranados N, Schwandt M, et al. Exome-wide association analysis identifies novel risk loci for alcohol-associated hepatitis. Hepatology. 2025;81(4):1304–17.
69. Gill D, Del Greco M F, Walker AP, Srai SKS, Laffan MA, Minelli C. The effect of iron status on risk of coronary artery disease: a Mendelian randomization study-brief report. Arterioscler Thromb Vasc Biol. 2017;37(9):1788–92.
70. Dennis A, Kelly MD, Fernandes C, Mouchti S, Fallowfield JA, Hirschfield G, Pavlides M, Harrison S, Chakravarthy MV, Banerjee R, Sanyal A. Correlations Between MRI Biomarkers PDFF and cT1 With Histopathological Features of Non-Alcoholic Steatohepatitis. Front Endocrinol (Lausanne). 2021;11:575843 https://doi.org/10.3389/fendo.2020.575843.


## Publisher's Note